ACS APPLIED MATERIALS & INTERFACES

Research Article

www.acsami.org

Self-Assembled Monolayers of Thiols Adsorbed on Au/ZnO-Functionalized Silica Nanosprings: Photoelectron Spectroscopy-Analysis and Detection of Vaporized Explosives

Blaise-Alexis Fouetio Kengne,*[,†] Saswata Karmakar,[‡] Mamta Kaura,[‡] V.V.R. Sai,[‡] Giancarlo Corti,[§] Ishwar B. Niraula,[†] Alexander Larin,[#] Jessica Hall,[#] Dewayne Sowell,[#] Patrick J. Hrdlicka,[‡] Vladimir Dobrokhotov,[#] and David N. McIlroy*[,†]

[†]Department of Physics, University of Idaho, Moscow, Idaho 83844-0903, United States

[§]School of Mechanical and Materials Engineering, Washington State University, Pullman, Washington 99164-2920, United States

[‡]Department of Chemistry, University of Idaho, Moscow, Idaho 83844-2343, United States

[#]Department of Physics and Astronomy, Western Kentucky University, Bowling Green, Kentucky 42101-1077, United States

Supporting Information

ABSTRACT: Self-assembled monolayers (SAMs) of thiols of L-cysteine, 6-mercaptohexanol, 4-mercaptobenzoic acid, DL-thioctic acid and 11-(1-pyrenyl)-1-undecathiol, which have been selected for their propensity to interact with vaporized explosives, have been attached from solution onto gold decorated ZnO-coated nanosprings. X-ray and ultraviolet photoelectron spectroscopies (XPS and UPS) have been used to investigate the surface electronic structure of the SAMs coated nanosprings. On the basis of XPS analysis, it has been determined that the packing densities of L-cysteine, 6-mercaptohexanol, 4-mercaptobenzoic acid, DL-thioctic acid and 11-(1-pyrenyl)-1-undecathiol on gold (zinc oxide) are 5.42×10^{14} (2.83×10^{14}), 3.26×10^{14} (2.54×10^{14}), 9.50×10^{13}, 2.55×10^{14} (1.12×10^{14}), and 5.23×10^{13} molecules/cm^2, respectively. A single S 2p core level doublet is observed for 4-mercaptobenzoic acid and 11-(1-pyrenyl)-1-undecathiol, which is assigned to the S−Au bond. The S 2p core level for L-cysteine, 6-mercaptohexanol, and DL-thioctic acid consist of two doublets, where one is S−Au bond and the other is the S−Zn bond. Analysis of the C/S ratios agrees well with the stoichiometry of the respective thiols. UPS analysis shows that the hybridization of S 3p states and Au d-bands produces antibonding and bonding states, above and below the Au d-bands, which is characteristic of molecular chemisorption on Au nanoparticles. Gas sensors were constructed with thiolated nanosprings and their responsiveness to ammonium nitrate at 100−150 °C was tested. Nanosprings sensors functionalized with 4-mercaptobenzoic acid and 6-mercaptohexanol showed the strongest responses by a factor of 4 to 5 relative to the less responsive thiols. The response to ammonium nitrate can be correlated to the packing density and ordering of the SAMs.

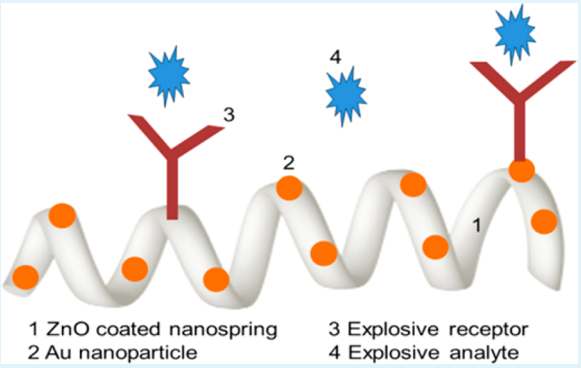

KEYWORDS: *nanosprings, thiols, chemisorption, photoemission, analytes*

1. INTRODUCTION

Generally speaking, sensors are designed to operate in an environment with predictable characteristics, such as an oxygen sensor in an automobile. Consequently, the sensor can be designed with a limited range of selectivity, which is exactly the case with the aforementioned example. Unfortunately, there are numerous applications, such as explosive detection, that are expected to operate in a variety of atmospheric conditions capable of producing false positives. Consider ammonium nitrate, a common fertilizer that is widely used and can produce a signature similar to that of the explosive TNT.[1,2] A gas sensor designed to detect TNT would have to be capable of differentiating airborne ammonium nitrate to the decomposition products of TNT. Chemical functionalization of the surface of the sensors with highly refined discrimination, i.e., selectivity, is the logical approach to develop sensors capable of distinguishing between naturally occurring chemical products and the anomalous chemical signature, for example, of an explosive.

Zinc oxide coated nanosprings are a high-surface-area nanomaterial that has been used to construct redox based sensors capable of detecting parts-per-billion concentrations of the explosives TATP and TNT in air,[3] and potentially parts-per-trillion concentrations. With the addition of a transition

Received: November 2, 2013
Accepted: July 14, 2014
Published: July 14, 2014

metal and precious metal nanoparticle coatings, the ZnO coated nanospring gas sensors are capable of producing electrical signatures that can be used to distinguish between acetone, ethanol, and toluene.[3] The drawback of using metal nanoparticles for producing an electrical signature specific to the redox of a target compound is the need for multiple sensors with different metal nanoparticles, parallel detection and analysis of the signals using linear discrimination analysis.[3] Ideally, one would prefer a sensor with a surface that is selective to one, and only one, chemical species. Self-assembled monolayers (SAMs) on metal nanoparticles, or semiconductors surfaces, are one approach to tailoring an interface with the desired specificity.[1,2,4−6] If the chemical detection of an analyte is via chemical bonding with the headgroup of the SAMs, which for the majority of cases will be irreversible, ZnO coated nanospring-based sensors will remain responsive to multiple low concentration analyte exposures due to their ∼200 m^2/g surface area, i.e., it will take numerous exposures to saturate the sensor surface before rendering the sensor unresponsive.

In the work reported herein, the electrical response and selectivity of SAMs functionalized Au nanoparticle decorated ZnO nanospring chemical sensors have been constructed and evaluated. The Au decorated ZnO-coated silica nanosprings have been functionalized with 6-mercaptohexanol, L-cysteine, 4-mercaptobenzoic acid, DL-thioctic acid and 11-(1-pyrenyl)-1-undecathiol. Note, the metal nanoparticle decorated ZnO nanospring sensors detect via redox, and subsequently operate at temperatures in excess of 300 °C. SAMs coated nanospring sensors, on the other hand, must be operated below the decomposition temperature of the SAMs layer and the electrical response of the sensor arises from interfacial charge accumulation due to bonding of the analyte to the headgroup of the thiol, or a change in the effective permittivity due to diffusion of the analyte into the SAM.[7] Critical to evaluating the electrical response is a thorough understanding of the bonding of the thiols on the Au nanoparticles and the ZnO surface of the nanosprings, ordering and packing density of the SAMs layers, as these will affect the accumulation of charge at the surface of the ZnO, and subsequently impact carrier transport along the nanosprings.[8,9] We also report on the thermal stability of the SAMs and the Au−S and Zn−S bonds, as determined with XPS and UPS. We have also used XPS to evaluate the packing density and order of the SAMs layers. These two factors are aligned with the ultimate goal of developing a nanospring-based sensor platform capable of selectively detecting vaporized explosives. Finally, we have evaluated the sensing responses of the SAMs coated nanospring sensors to a variety of explosive vapors and solvents. We have attempted to correlate the effects of SAMs bonding to the Au nanoparticles and ZnO surface, ordering and packing density of SAMs layers, the electronic structure of the SAMs/nanospring interfaces, and the SAMs headgroups with sensor responses and selectivity. Ultimately, the desired outcome is to identify the most critical of the aforementioned variables in relation to sensor selectivity and response.

2. EXPERIMENTAL DETAILS

2.1. Sample Synthesis. *2.1.1. Synthesis of Nanospring-mats, Coating, and Decoration.* The process for producing mats of nanosprings and their coating with ZnO by atomic layer deposition (ALD) have been discussed in detail in ref 9. The ZnO-coated silica nanosprings were decorated with gold nanoparticles by reducing gold(III) chloride ($AuCl_3$) to metallic gold through a pyrolysis-like process. A 19.5 mM solution was prepared by dissolving $AuCl_3$ in deionized water. The solution was subsequently mixed with 20% reagent grade ethanol to improve solvent evaporation and the nucleation of Au nanoparticles. The samples were dipped in the solution and dried in air at room temperature. Subsequently, they were baked in a preheated tube furnace at 300 °C at atmospheric pressure under Ar/H_2 flow of 480 sccm/38 sccm for 15 min. In the last step, the samples were allowed to cool down to room temperature in an Ar atmosphere to minimize condensation of water. A field emission scanning electron microscope (FESEM) micrograph of a Au/ZnO nanosprings sample is shown in Figure 1. Although not visible in Figure 1, the silica nanosprings

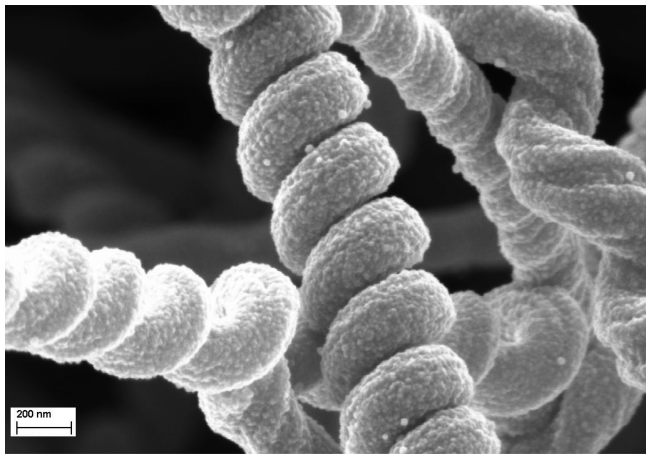

Figure 1. FESEM micrographs of silica nanosprings coated with ZnO and subsequently decorated with Au nanoparticles, where the morphology of the nanosprings is retained after coating. The granular structure of the coating consists of ZnO and Au nanoparticles.

consist of five to eight intertwined silica nanowires.[10] The ALD grown ZnO coating is highly conformal to the underlying nanosprings and granular in nature, with an average grain size of 20 nm, in excellent agreement with the value of (18 ± 3) nm calculated from X-ray diffraction (XRD) data (not shown). The Au nanoparticles are not distinguishable from ZnO crystallites in the FESEM image due to absence of sufficient contrast. We could not rely on the XRD data for particle size calculation given the significant contribution of the underlying Au catalyst used for nanospring synthesis to the Au signal. We therefore used TEM micrographs (not included here), where the mean particle size was measured to be (10 ± 4) nm.

2.1.2. Molecular Functionalization. A total of five Au/ZnO-coated silica nanospring mats (area ∼1 cm^2 grown on a Si wafer) were prepared and functionalized with either 6-mercaptohexanol, L-cysteine, 4-mercaptobenzoic acid, DL-thioctic acid, or 11-(1-pyrenyl)-1-undecathiol (selected for their propensity to interact with vaporized explosives)[1,4,6] through incubation of the mats with 10 mM of the selected thiol in an appropriate solvent (6-mercaptohexanol, 4-mercaptobenzoic acid, and DL-thioctic acid in ethanol, L-cysteine in DI water, and 11-(1-pyrenyl)-1-undecathiol in toluene) for 48 h to allow uniform and dense SAM formation. The substrates were subsequently washed thrice in the respective solvents and dried under a stream of argon. Highly concentrated thiol solutions were required, as compared to 10 μM solutions typically used when functionalizing flat gold surfaces, due to high surface area of ZnO coated nanospring

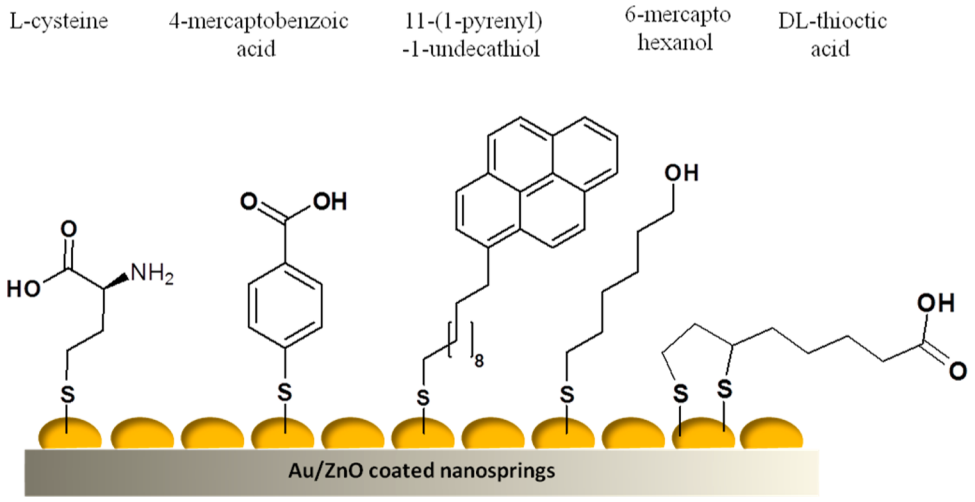

Figure 2. Illustration of idealized binding of thiol groups to the surface of Au/ZnO-coated nanosprings.

mats (~200 m^2/g). 11-(1-pyrenyl)-1-undecathiol was synthesized following the protocol in Supporting Information, part II. Figure 2 illustrates the anticipated surface attachment of the thiols to the surface of the Au nanoparticles.

2.2. X-ray and Ultraviolet Photoelectron Spectroscopies (XPS and UPS). Photoelectron spectroscopic analysis of the thiolated nanosprings was performed in a custom built ultrahigh vacuum (UHV) chamber with a base pressure of 1.5×10^{-10} Torr. The chamber is equipped with an Omicron model EA 125 hemispherical electron energy analyzer, a dual anode X-ray source, and a He UV lamp. Both the X-ray source and the UV lamp are at the so-called magic angle of 54.7° relative to the axis of the electron analyzer. The MgKα emission line (1253.6 eV) was used for all XPS data acquisition. Given the highly disordered nature of the nanospring samples (randomly oriented nanosprings and a mat thickness of ~60 μm), in conjunction with the specifications of the X-ray source and electron analyzer, the upper resolution of the XPS spectra is estimated to no better than 300 meV, as determined by the full width at half-maximum (fwhm) of the Au $4f_{7/2}$ core level state of the bare Au/ZnO nanospring sample. To avoid spurious charging, the sample was grounded and exposed to a 153 eV electron beam using an electron flood gun. Note, dissociation of the thiols directly by the primary electrons of the flood gun, or subsequent low energy secondary electrons, with extended exposure was not observed. The data pertaining to the use of the electron flood gun is available in the Supporting Information, part I. Binding energies reported herein are referenced to the C 1s peak at 285 eV. UPS spectra were acquired with the He I line (21.2 eV) from a Specs UVS 10/35 source, using ultrapure He (99.999%) that was passed through a liquid nitrogen cold trap. The Fermi edge of a polycrystalline Au specimen was used for binding energy calibration. In both experiments the takeoff angle was 90°, corresponding to photoelectron emission normal to the sample surface. All spectra were acquired at room temperature. The fitting of the XPS spectra consisted of subtracting a Shirley background prior to peak fitting with Voigt functions.

2.3. Gaseous Analyte Detection Measurements. The apparatus for sensor measurements, as well as test protocols, are described in detail in ref 9. Briefly, a standard two-electrode was used for measuring the electrical response of the samples to chemical vapors. The sensor was connected to a thermocouple and placed on a variable temperature platform for temperature control. The sensor responses were acquired with a Keithley 2400 source-sense meter interfaced to a computer via Labview operated data acquisition software allowing for real time conductance measurements. The sensor was initially heated to the desired temperature. When a steady state resistance was obtained, pulses of vapor were produced by a VaporJet calibrator. Liquid analytes were evaporated while solids were sublimated. The VaporJet's ability to sublimate solids almost instantly allows for extremely short pulses on the order of milliseconds. Sensors were tested with vapors of ammonium nitrate (NH_4NO_3), 2,4-dinitrotoluene (DNT), acetone, toluene, and ethanol, which are explosives or degradation products of explosive compounds. The experiments were carried out at 100 or 150 °C, which is below the maximum desorption temperature of the SAMs, as verified by the XPS analysis (see the Supporting Information, part I).

3. RESULTS AND DISCUSSION

3.1. X-ray Photoelectron Spectroscopy (XPS). Broad survey XPS scans of the five SAM-functionalized Au/ZnO nanosprings samples exhibited core level states of Au (4f), C (1s), Zn (3d, 3p, 3s, 2p), O (1s), and S (2s, 2p) (not shown). The sulfur signal of 11-(1-pyrenyl)-1-undecathiol was very weak, where the weakness is attributed to a different molecular coverage relative to the other thiols as a result of its long hydrophobic chain. The L-cysteine functionalized sample also included a N (1s) core level state associated with the amine group ($-NH_2$). To investigate the chemical environment of Au, C, S, O, Zn, and N, we acquired higher resolution scans of these core levels. Figure 3 shows the overlapping Au 4f and Zn 3p core level states.

Quantitative analysis of the XPS spectra of the untreated Au/ZnO sample indicates an atomic ratio of Au/Zn of 0.05. The binding energy of Au 4f for the treated samples is in agreement with results reported for these thiols assembled on gold nanoparticles.[7−11] For peak fitting of the spectra in Figure 3, the spin−orbit splitting of Au 4f was held at 3.65 eV and the ratio of the Au $4f_{7/2}$:Au $4f_{5/2}$ intensity held at 4:3. The Au 4f binding energy shifts to higher binding energies with thiol functionalization relative to the pristine Au/ZnO nanosprings sample, with the exception of 4-mercaptobenzoic acid. This is

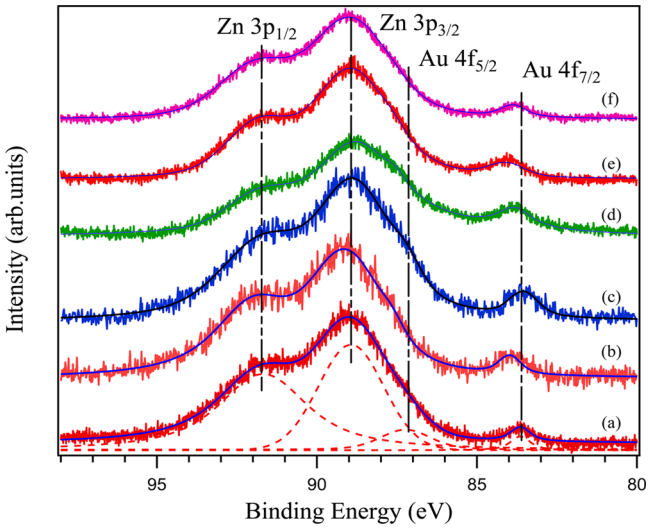

Figure 3. Au 4f-Zn 3p core level states of (a) an untreated Au/ZnO sample and samples treated with (b) DL-thioctic acid, (c) 4-mercaptobenzoic acid, (d) L-cysteine, (e) 6-mercaptohexanol, and (f) 11-(1-pyrenyl)-1-undecathiol.

indicative of charge redistribution associated with the formation of the S−Au bond between the thiols and the Au nanoparticles.

Treated samples contain a substantial amount of carbon due to the organic thiols. In order to achieve a satisfactory peak fitting, the adventitious carbon, as detected from the untreated sample, was included in the deconvolution of C 1s spectra. The position of a photoelectron peak is sensitive to the charge density on the un-ionized atom and to the degree of shielding of the core-hole generated by the loss of the electron. For C 1s, this sensitivity manifests itself as chemical shifts to higher binding energies for carbons in higher oxidation states or with electronegative substituents.[12] The peaks at 284.79 eV (L-cysteine), 284.80 eV (6-mercaptohexanol), 284.97 eV (11-(1-pyrenyl)-1-undecathiol), and 284.88 eV (DL-thioctic acid) are assigned to the C−C/C−H bonds of the aliphatic carbons in the respective thiols. The peak at 285.33 eV (6-mercaptohexanol) corresponds to C−S. The aromatic carbons are the singlets at 284.44 eV (11-(1-pyrenyl)-1-undecathiol) and 284.42 eV (4-mercaptobenzoic acid) because a chemical shift of ∼0.5 eV occurs in the aromatic species relative to aliphatic unfunctionalized carbon atoms.[13] The contribution at a binding energy of ∼286 eV is characteristic of C−S, C−O, or C−N bonds. Signals between 288 and 289 eV are assigned to carbon species involved in the carboxylic acid functional group (O═C−O) of L-cysteine, 4-mercaptobenzoic acid, and DL-thioctic acid. These assignments are summarized in Table 1.

The S 2p signal was fitted with two or four peaks, which correspond to one doublet (S $2p_{3/2}$, S $2p_{1/2}$) or two sets of doublets (see Figure 5). The fitting procedure of the S doublet consisted of using the same fwhm for both spin states, holding the spin−orbit splitting at 1.2 eV, and a branching ratio of 2:1 (S $2p_{3/2}$:S $2p_{1/2}$). The lower binding energy S doublet is ascribed to sulfur bound to Au. The second doublet is attributed to unbound free thiol groups, and/or bonding of the headgroup instead of S[16] or a S−Zn bond.[18] In the present work, the second doublet is attributed to the S−Zn bonds because alkanethiols are known to form monolayers on ZnO surfaces through S−Zn bonding.[16,18−21] A peak at 170 eV, which corresponds to an S−O bond, was not observed. The conclusion is that thiol bonding is either to Au or Zn sites. The

Table 1. Results of the Deconvolution of the C 1s Spectra from Figure 4

sample	binding energy (eV)	assignment	ref
L-cysteine	284.79	C−C, C−H	14
	285.99	C−N, C−O or C−S	15,16
	288.39	O═C−O	13
6-mercaptohexanol	284.80	C−C, C−H	14
	285.33	C−S	16
	286.43	C−O	17
11-(1-pyrenyl)-1-undecathiol	284.44	aromatic carbon	13
	284.97	C−C, C−H	13
	285.92	C−S	16
DL-thioctic acid	284.88	C−C, C−H	14
	285.99	C−O, C−S	16
	288.39	O═C−O	13
4-mercaptobenzoic acid	284.42	aromatic carbon	13
	284.72	C−C, C−H	14
	285.99	C−O, C−S	16
	288.90	O═C−O	13

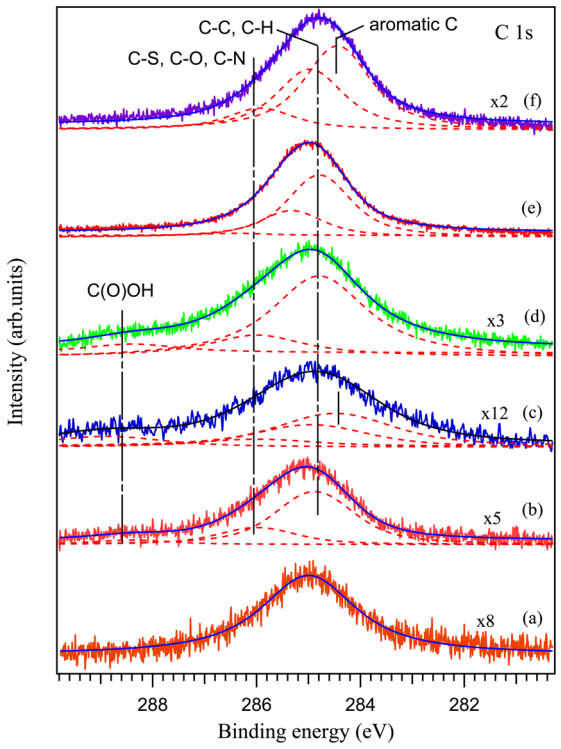

Figure 4. C 1s core level states of (a) an untreated Au/ZnO sample and treated with (b) DL-thioctic acid, (c) 4-mercaptobenzoic acid, (d) L-cysteine, (e) 6-mercaptohexanol, and (f) 11-(1-pyrenyl)-1-undecathiol.

weakness of the sulfur signals of 4-mercaptobenzoic acid and 11-(1-pyrenyl)-1-undecathiol samples reflects the attenuation of the signal due to enhanced photoelectron scattering off of the aromatic ring(s), or possibly a higher degree of disorder within these SAMs. Steric hindrance in 4-mercaptobenzoic acid and 11-(1-pyrenyl)-1-undecathiol SAMs is expected due to aromatic rings in the headgroup, resulting in greater attenuation of the sulfur photoelectrons. This is supported by work by Bain et al.,[12] who reported a weak sulfur signal in the XPS characterization of the following thiols on gold: HS-$(CH_2)_{10}CH_3$, $HS(CH_2)_{10}CH_2OH$, $HS(CH_2)_{10}CO_2H$, HS-

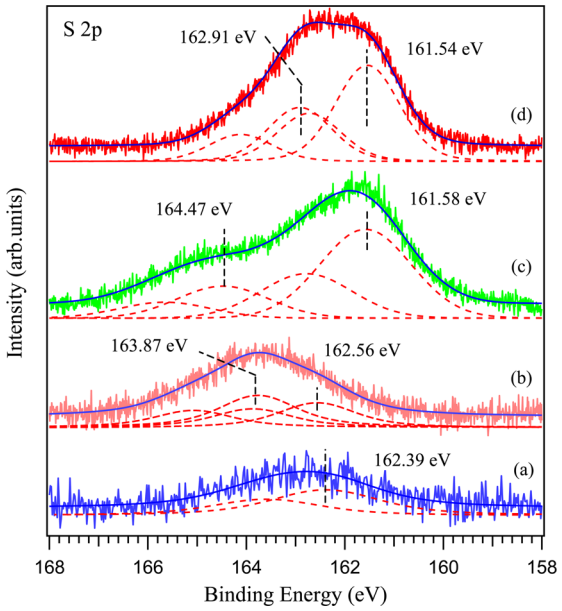

Figure 5. S 2p core level states of (a) 4-mercaptobenzoic acid, (b) DL-thioctic acid, (c) L-cysteine, and (d) 6-mercaptohexanol treated Au/ZnO nanospring samples. The peaks were fitted using one or two doublets corresponding to two different sulfur bonds.

$(CH_2)CO_2CH_3$, $HS(CH_2)_{10}CH_2Cl$, and $HS(CH_2)_8CN$. They invoked monolayer orientation to explain the inelastic scattering of the S 2p electrons by the molecules within the monolayer. Given the spherical to semihemispherical shape of Au nanoparticles on 1D nanostructures,[22,23] one expects a higher degree of random tilting of 4-mercaptobenzoic acid and 11-(1-pyrenyl)-1-undecathiol relative to the photoelectron takeoff angle, as compared to a planar Au surface.

Displayed in Figure 6 are the O 1s spectra of the untreated and thiolated Au/ZnO nanosprings, which are fitted with two to three components. The peak at ∼530 eV (O_l) is due to the

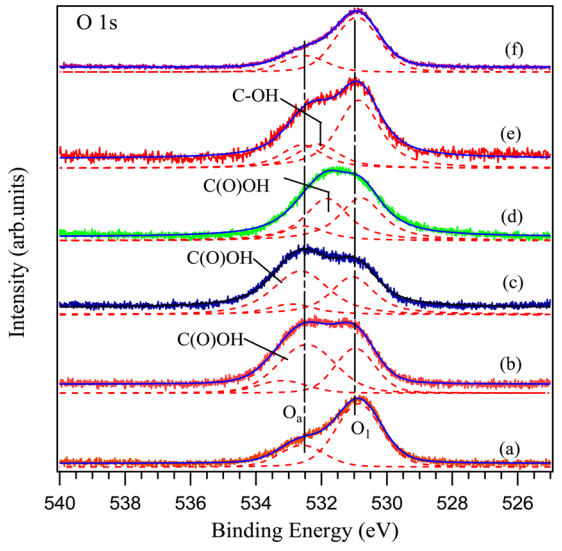

Figure 6. O 1s core level states of an (a) untreated Au/ZnO sample and samples treated with (b) DL-thioctic acid, (c) 4-mercaptobenzoic acid, (d) L-cysteine, (e) 6-mercaptohexanol, and (f) 11-(1-pyrenyl)-1-undecathiol. O_l represent O^{2-} in the wurtzite structure of ZnO and O_a chemisorbed oxygen.

lattice oxygen in ZnO, which is in the O^{2-} state, whereas the peak at ∼532.7 eV (O_a) originates from hydroxyl groups or chemisorbed oxygen.[24,25] The O 1s core level state for 11-(1-pyrenyl)-1-undecathiol treated nanosprings is virtually unchanged relative to the untreated nanospring sample, indicating that it does not bond to the ZnO surface. The significant change observed in the spectra of the other thiolated samples is due to large contributions from the COOH and/or OH groups within the thiols. Maintaining a fixed ratio between O_l and O_a allowed us to resolve these contributions. It can be seen that the chemisorbed oxygen shoulder is mainly affected, which indicates that those functional groups are located at the top surface of the monolayer.

The binding energy of the Zn $2p_{3/2}$ and Zn $2p_{1/2}$ core level states (Figure 7) are at ∼1022 eV and ∼1045 eV, respectively,

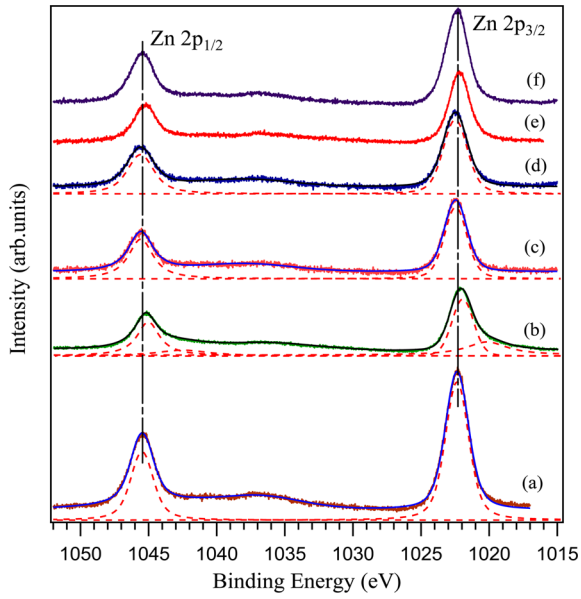

Figure 7. Zn 2p core level states of (a) an untreated Au/ZnO nanospring sample and treated with (b) L-cysteine, (c) DL-thioctic acid, (d) 4-mercaptobenzoic acid, (e) 6-mercaptohexanol, and (f) 11-(1-pyrenyl)-1-undecathiol.

consistent with ZnO. The peak position for Zn $2p_{3/2}$ is in good agreement with the wurtzite phase of ZnO at 1022.4 eV.[26] The absence of a metallic zinc peak at 1021.5 eV indicates that the ionization state of Zn is Zn^{2+}.[24] There is a very small spectral contribution on the lower binding energy side of the L-cysteine treated sample that likely arises from the electrostatic interaction between Zn^{2+} ions and the electrically charges sites of L-cysteine ($-COO^--$) and ($-NH_3^+-$) when L-cysteine exists in the zwitterionic form. Alternatively, it could be attributed to S−Zn bonds. However, the latter is less likely since the four other thiols have been grafted following the same protocol, and the S−Zn bond therefore should have appeared in the Zn 2p core level states of all the samples. The attenuation of the Zn 2p photoelectrons upon treatment, in conjunction with the peaks assignment of the S 2p core level states, demonstrates the formation of thiol overlayers on the ZnO surfaces.

The N 1s core level state for L-cysteine is shown in Figure 8. The single peak at ∼400 eV corresponds to NH_x species.[14] The N 1s signal provides confirmation for the location of the headgroup at the top surface of the monolayer. Signals from

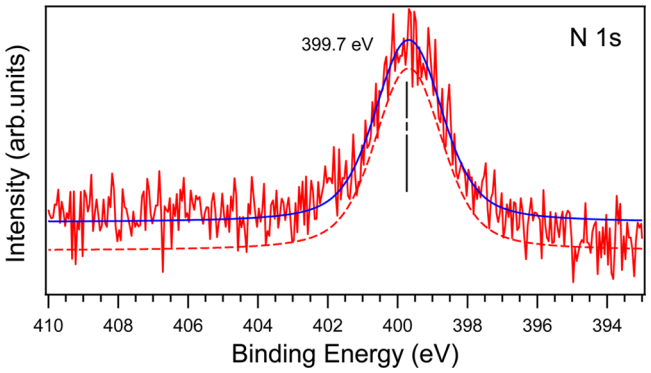

Figure 8. N 1s core level for L-cysteine functionalized Au/ZnO nanospring sample.

oxidized nitrogen species (NO_x) at higher binding energies were not observed, indicative of the stability and resistance of L-cysteine to oxidation.

Table 2 summarizes the atomic ratios of the elements calculated from the integration of the XPS core level states, which were corrected by Scofield sensitivity factors obtained from the literature.[27,28] The area of carbon impurities, as detected in the untreated sample, were subtracted from the area of each C 1s core level prior to the elemental analysis.

The carbon to sulfur ratios (C 1s/S 2p) are close to the expected theoretical values corresponding to the stoichiometry of the linker molecules, which confirm the quality of monolayers and the reliability of the sensitivity factors used. The Au/Zn ratios reflect the low content of Au in the samples. Compared with the value of 0.05 for the untreated sample, the relative decrease (except for 4-mercaptobenzoic acid) provides additional evidence of a monolayer on the Au nanoparticles. For 4-mercaptobenzoic acid the change is likely due to differences in chemical interactions with Au/ZnO and molecular orientation. The S 2p/Au ratios follow the trend of the S 2p signal detected from the respective samples, but the values should not be much greater than unity if sulfur binds exclusively to Au. Conversely, the S 2p/Au+Zn ratios are more reasonable, consistent with chemisorption via S−Au and S−Zn bonds.

The nature of the interface between Au/ZnO nanosprings and the adsorbed thiols is an important point of interest. X-ray absorption near-edge spectroscopy (XANES) studies of thiol-capped ZnO nanoparticles have demonstrated the existence of a ZnS-ZnO interface at the surface of the nanoparticles, with both ZnS and ZnO showing a wurtzite structure.[29−31] The S 2p core level states from L-cysteine, 6-mercaptohexanol, and DL-thioctic acid treated samples clearly exhibited two sulfur signals, which are assigned to S−Au, and S−Zn bonds. For 11-(1-pyrenyl)-1-undecathiol and 4-mercaptobenzoic acid) the S−Au bond is dominant.

Packing Density and Order/Disorder of SAMs. Packing densities of thiols are calculated from the XPS data following the method described in ref 32. Because XPS probes only a few atomic layers of the sample, to estimate the packing density of thiols on nanoparticles XPS integrals must be corrected for the electron escape depth ($\lambda\cos\theta$), where λ is the inelastic mean free path (IMFP) and θ the emission angle to the surface normal. For normal emission, as in our experiments, the escape depth reduces to simply λ. From the NIST Electron Inelastic Mean Free Path Database, the IMFPs of gold and zinc are 1.78 and 2 nm, respectively.[27]

The shell method models nanoparticles as a central atom surrounded by shells (layers) of atoms, where the number of atoms in the nth shell is $10n^2 + 2$.[32] The total number of shells can then be determined from the diameters of the atoms and the nanoparticles. The number of layers sampled by XPS is the ratio of the escape depth to the atom diameter. From these estimates, a 10 nm gold nanoparticles contains 18 shells, where only 6 are probed by XPS, whereas zinc nanoparticles of 7 nm (size of coordinated zinc in a 18 nm ZnO crystal) contain14 shells, of which 8 are sampled.

The S to Au or to Zn atomic ratios are corrected as follows

$$\frac{S}{X_{\text{surface}}} = \left(\frac{\sum_{n=n_i}^{n_o}(10n^2+2)}{10{n_o}^2+2}\right)\left(\frac{S}{X}\right);\quad X = \text{Au, Zn} \tag{1}$$

where n_i is the deepest layer sampled and n_o the outer layer. The surface of a 10 nm gold nanoparticles mostly contains (100) crystal planes.[32] Large-grain ZnO (~20 nm) correspond to the growth mode with the c-axis parallel to the substrate with 100 and 110 orientations, or predominantly (100) surface planes.

The number of lattice points per unit area of a crystal plane is given by

$$\rho_{hkl} = \frac{nd_{hkl}}{\Omega} \tag{2}$$

where n is the number of lattice points per unit cell, Ω the volume of the unit cell, and d_{hkl} the interplanar spacing.

The packing density of atoms on a plane (σ_{hkl})is calculated as follows

$$\sigma_{hkl} = N_0\rho_{hkl} \tag{3}$$

where N_0 is the number of atoms per lattice point in the plane (hkl). These quantities for Au and Zn are

$$\sigma_{hkl}(\text{Au}) = \frac{2}{a^2(h^2+k^2+l^2)^{1/2}} \tag{4}$$

and

Table 2. Atomic Ratios of Elements at the Outer Surface of Treated Samples

	C 1s/S 2p					
sample	theoretical	XPS	S2p/Au	Au/Zn	S2p/Zn2p + Au	C1s + S2p/Zn2p + Au
L-cysteine	1.12	1.40	46.06	0.014	0.64	2.09
6-mercaptohexanol	2.25	2.22	58.59	0.018	1.01	4.38
11-(1-pyrenyl)-1-undecathiol	10.5	10.1	5.88	0.028	0.16	2.59
4-mercaptobenzoic acid	2.62	2.47	6.59	0.057	0.36	1.69
DL-thioctic acid	1.50	1.42	64.73	0.028	1.17	3.67

Table 3. Surface Coverage and Packing Density (PD) of Thiols on Au and Zn as Determined by XPS

thiols	L-cysteine	6-mercaptohexanol	11-(1-pyrenyl)-1-undecathiol	DL-thioctic acid	4-mercaptobenzoic acid
coverage on Au	0.451	0.271	0.0435	0.106	0.0791
PD on Au (molecules/cm^2)	5.42×10^{14}	3.26×10^{14}	5.23×10^{13}	2.55×10^{14}	9.50×10^{13}
coverage on Zn	0.239	0.215		0.0475	
PD on Zn (molecules/cm^2)	2.83×10^{14}	2.54×10^{14}		1.12×10^{14}	

$$\sigma_{hkl}(Zn) = \frac{2}{\sqrt{3}\,a^2 c\left(\frac{4}{3}\frac{h^2+hk+k^2}{a^2} + \frac{l^2}{c^2}\right)^{1/2}} \quad (5)$$

Finally, the packing density of thiols can be approximated from XPS data using the following relationship

$$\mathrm{PD} = \left(\frac{S}{X_{\mathrm{surface}}}\right)\left(\frac{TH}{S}\right)(\sigma_{hkl}) \quad (6)$$

The factor TH/S is 2 for DL-thioctic acid and 1 for the other thiols in this study. The surface coverage and packing density calculated by the above method are summarized in Table 3.

The values agree with the SAMs packing densities on flat gold surfaces of the order of 1×10^{14} molecules/cm^2.[33] L-cysteine, 6-mercaptohexanol, and DL-thioctic acid are more densely packed than 4-mercaptobenzoic acid and 11-(1-pyrenyl)-1-undecathiol. The latter thiols have larger end groups, where the reduced packing densities may be due to steric hindrance.

We believe that ordering of the thiols is a very important factor in terms of sensor response, where response is directly related to the effectiveness of the receptors, i.e., the headgroups need to be accessible to the surrounding atmosphere to increase the probability of coming in contact with the analyte, particularly at low concentrations. It has been reported for 4-mercaptobenzoic acid that the proximity of the carboxyl group to the surface of the monolayer—compared to similar types of thiols—reduces its interaction with the substrate, resulting in an increased reactivity with vapors of analytes.[34,35] SAMs of DL-thioctic acid formed in ethanol are highly disordered due to hydrogen bonding between neighboring molecules with a tilt of 38° that results in the loose packing of the SAM.[36] Unlike DL-thioctic, the higher degree of ordering of 6-mercaptohexanol SAMs is ascribed to complementary effects, such as the solubility of solvents with the thiol chains and hydrogen bonding of adjacent −OH of thiols or −OH with solvents.[37] Note, a high packing density is required to order long-chain molecules within a monolayer;[38] and for SAMs of 11-(1-pyrenyl)-1-undecathiol with an increased steric hindrance of the headgroups, they are likely to be disordered. Finally, SAMs of L-cysteine are highly ordered, most likely because of intermolecular and intramolecular interactions of hydrophilic ammonium and carboxylic groups that lead to the formation of hydrogen bonds between adsorbed molecules.[39]

3.2. Ultraviolet Photoelectron Spectroscopy (UPS).

UPS spectra (He I emission line) of a bare ZnO nanospring, untreated Au/ZnO nanosprings and the five thiol-treated Au/ZnO nanosprings are displayed in Figure 9 (upper panel). The spectrum of the untreated sample is reminiscent of polycrystalline Au and ZnO valence bands with some attenuation and hybridization. The Au 5d electrons form a broad band between 2 and 8 eV and the 6s band is observed between the Fermi level and 2 eV. Note, the 6s band extends to much higher binding energy and is strongly hybridized with the 5d bands.[40] As for ZnO, the valence band extends from 3 to 8 eV; theory predicts

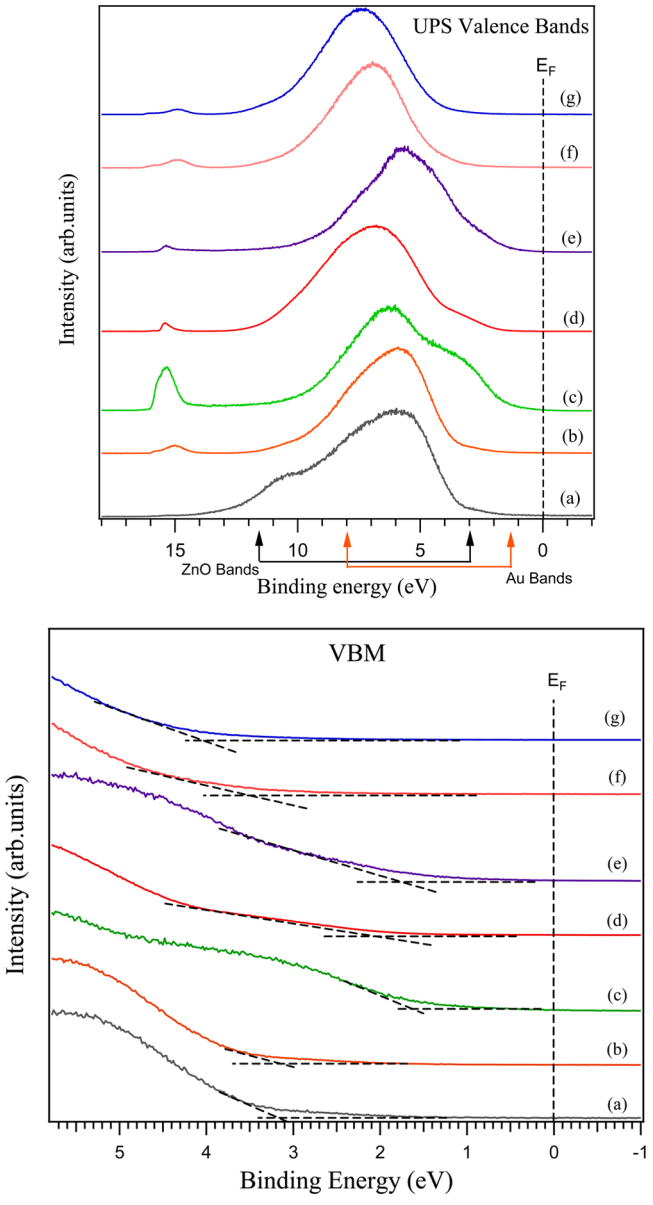

Figure 9. (Upper panel) UPS (He I) valence bands spectra for (a) a bare ZnO nanospring-mat, (b) an untreated Au/ZnO nanospring-mat and (c) treated with L-cysteine, (d) 6-mercaptohexanol, (e) 11-(1-pyrenyl)-1-undecathiol, (f) DL-thioctic acid, and (g) 4-mercaptobenzoic acid. (Lower panel) The valence band maxima (VBM) of the same samples obtained by linear extrapolations.

that the emission from 3 to 5 eV corresponds to nonbonding O 2p orbitals, and between 5 and 8 eV to hybridization of the O 2p and Zn 4s orbitals.[41] The Zn 3d band at 10 eV of the valence band spectra of bare ZnO is attenuated upon decoration with Au nanoparticles. Duwez et al.[42] noted that one of the difficulties one encounters when interpreting valence band spectra consisting of Au and organics is the super-

Table 4. Position of the VBM of Thiol-Treated Au/ZnO Nanospring Surfaces

	sample treated with				
	L-cysteine	11-(1-pyrenyl)-1-undecathiol	6-mercaptohexanol	4-mercaptobenzoic acid	DL-thioctic acid
VBM (eV)	1.50	1.45	1.80	3.10	3.05

imposition of the Au 5d signal with the valence band structure of the organic material. There are, however, obvious changes to the shape of the Au/ZnO spectrum upon thiol functionalization. For instance, the Au 5d and Zn 4s-O 2p bands are attenuated differently. For DL-thioctic acid and 4-mercaptobenzoic acid functionalization these bands are almost completely suppressed, yet still resolvable upon functionalization with L-cysteine, 6-mercaptohexanol and 11-(1-pyrenyl)-1-undecathiol. These changes are indicative of thiol bonding to Au and Zn surface sites.[42] The thickness and compactness of the film will affect the intensity of photoemission from the underlying substrate, where the analysis of the XPS spectra demonstrated that the packing density of the thiols on the Au nanoparticles differ from that on the ZnO surface. Note, the presence, or absence, of contributions from Au and ZnO in the valence spectra can be related to the hydrocarbon chain length, the size of the end group, and the molecular orientation of the thiol. Finally, the feature at ~15 eV is the background of secondary electrons that arise from the substrate near-surface region, as well as the thiol layer.[43]

Included in Figure 9 (lower panel) are linear extrapolations of the leading edges of the valence bands to obtain the VBM of the different thiolated surfaces (see also Table 4). Band bending (initial state) and dipole layer formation (final state) lead to energy shifts in the VBM (band bending) and, electron binding energies of the substrate states and molecular orbitals of the thiols.[43]

Difference spectra analysis of the valence band spectra in Figure 9 (upper panel) has been performed to elucidate the changes in the valence band density of states of the five thiols. The procedure is described in detail in ref 44. The results for all five thiols are summarized Figure 10. Negative features in the difference curve arise from suppression of valence band density of states of the Au/ZnO nanosprings, where attenuation is attributable to either electron scattering arising from disorder in the thiol layer or hybridization of S and Au surface atoms. The negative features at a binding energy of ~5 eV in the difference curves of L-cysteine, DL-thioctic acid and 4-mercaptobenzoic acid correspond to thiol suppressed Au d-bands. The attenuation of the Au d-bands with DL-thioctic acid functionalization and the lack of molecular orbitals of DL-thioctic acid are attributed to electron scattering due to disorder within the layer (see section 3.1). The difference spectrum of 4-mercaptobenzoic acid, taken in conjunction with its low coverage (Table 3), suggests that the attenuation of the Au feature is due to hybridization of S with the Au surface, as opposed to electron scattering. The molecular orbitals of 4-mercaptobenzoic acid in the range of ~6−12 eV support this conclusion. The new density of states in the range of 1−2 eV for L-cysteine, 11-(1-pyrenyl)-1-undecathiol, and 6-mercaptohexanol is attributed to hybridization of the antibonding S 3p-states with the Au 5d-bands, where the new states at binding energies >2 eV are the molecular orbitals of the respective thiols. In the case of L-cysteine, there is a contribution from N 2p state above 1.5 eV.[45] Note, the assignments are based on the assumption that the S antibonding 3p orbital does not mix with the wave functions on the hydrocarbon chain. The formation of

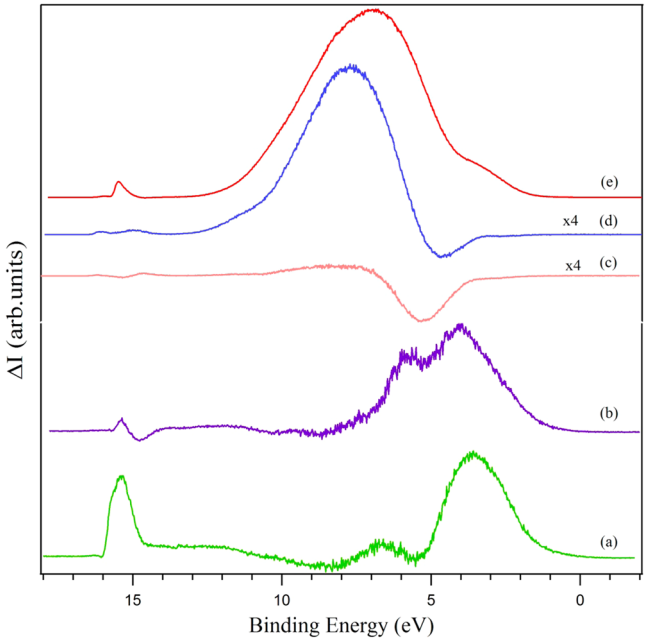

Figure 10. UPS difference spectra for chemisorbed (a) L-cysteine, (b) 11-(1-pyrenyl)-1-undecathiol, (c) DL-thioctic acid, (d) 4-mercaptobenzoic acid, and (e) 6-mercaptohexanol on Au/ZnO nanosprings.

hybrid orbitals of both bonding and antibonding type above and below the metal d bands, is consistent with the Newns−Anderson model for atomic and molecular chemisorptions on metal surfaces.[46] This is observed in the difference spectrum of L-cysteine and is in agreement with Felice and co-workers[47] application of the Newns−Anderson model to theoretically predict the band structure of cysteine chemisorbed on Au (111). The bonding and antibonding orbitals are both π-like and σ-like. In the higher binding energy region of the valence band between ~6−12 eV, bands are attributed to thiol C 2p orbitals states, as well as N 2p orbital state in the case of L-cysteine. These orbitals also contribute to the bonding of the molecules to the surface, especially the ZnO surface, where bonding primarily occurs via high-lying orbitals.[48]

3.3. Gaseous Analyte Detection Properties. The electrical response of thiol functionalized Au/ZnO nanospring sensors to the presence of explosive analytes are summarized in Figure 11. The electrical responses are in terms of the relative change in conductance relative to the baseline signal in the absence of vapor, and are subsequently normalized to the baseline.

The sensors must be operated at elevated temperatures in order to thermally activate carriers in the ZnO.[49] It has been reported that the heating of monolayers of alkanethiols on gold begin desorbing above 70 °C, but that the rate of desorption is dependent on the temperature, ambient medium, and chain length of the adsorbate.[12] Desorption is most rapid in a hydrocarbon solvent, slower in ethanol and in air. Long-chain thiols form monolayers that are more stable than those of short-chain thiols. However, the typical operating temperature

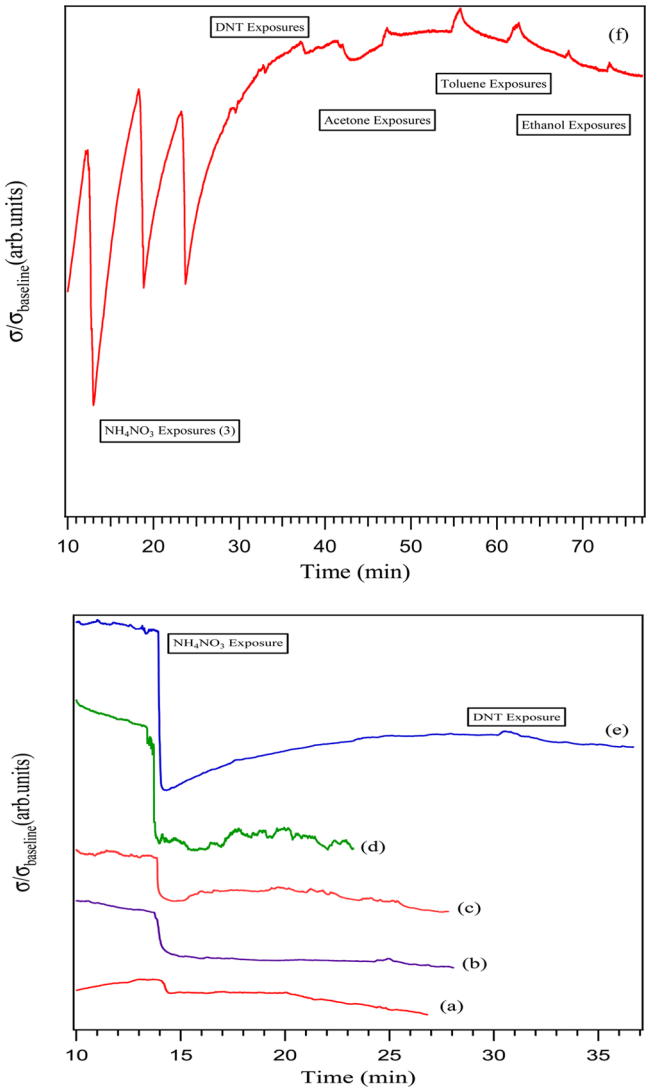

Figure 11. Relative change in conductance of (a) untreated Au/ZnO nanospring-mat and samples treated with (b) 11-(1-pyrenyl)-1-undecathiol, (c) DL-thioctic acid, and (d) L-cysteine upon exposure to ammonium nitrate, (e) 4-mercaptobenzoic acid, and (f) 6-mercaptohexanol upon exposure to ammonium nitrate, DNT, acetone, toluene, and ethanol.

of ZnO nanospring chemiresistors is 400 °C, which is expected to exceed the stability of SAMs. Consequently, it has been necessary to evaluate the thermal stability of the thiol layers on Au/ZnO nanosprings. The stability of thiol layers was evaluated by monitoring their XPS spectra as a function of annealing (see the Supporting Information, part I). It has been determined that the 11-(1-pyrenyl)-1-undecathiol and DL-thioctic acid functionalized sensors are safe to operate at 100 °C without damaging or desorbing the thiol layers, and 150 °C for the other thiol functionalized sensors.

Figure 11 demonstrates that the linker molecules were much more thermally stable than those adsorbed on gold, where it is hypothesized that bonding to ZnO surfaces stabilizes the SAMs. All of the thiolated sensors exhibited greater response to ammonium nitrate (NH_4NO_3) relative to the untreated Au/ZnO nanospring sensor. All of the sensors when exposed to NH_4NO_3, regardless of functionalization or lack thereof, exhibited a decrease in conductance. For all but the 6-mercaptohexanol, the responses were irreversible. Furthermore, the 6-mercaptohexanol functionalized sensor also subsequently responded reversibly to 2,4-dinitrotoluene (DNT), toluene, acetone, and ethanol. Interestingly, when the 6-mercaptohexanol functionalized sensor is exposed to liquid (solid) analyte the conductance increases (decreases). It has been suggested that the increased conductance of sensors constructed with porous films upon exposure to vapor from liquid analytes is a consequence of diffusion into the pores of the film.[7] The physical explanation is that vapors occupying the pores increases the average permittivity, which in turn increases the conductance by lowering the activation energy and height of the potential well barriers to carrier transport.[7] The self-refreshing characteristic of the 6-mercaptohexanol functionalized sensor (Figure 11) is indicative of analyte adsorption and subsequent desorption, i.e. not chemisorption. The reversibility of the 6-mercaptohexanol may be a reflection of the highly ordered nature of this SAM layer and the ability of the analyte to diffuse in and out the SAM.

4-mercaptobenzoic acid and 6-mercaptohexanol exhibited the strongest responses by a factor of 4 and 5 relative to 11-(1-pyrenyl)-1-undecathiol, the least responsive thiol. One might hypothesize that the large response of 4-mercaptobenzoic acid and 6-mercaptohexanol functionalized sensors is due to larger thiol-induced surface band bending of the ZnO, which upon exposure to the analyte induces corresponding larger charge redistribution within the ZnO. However, examination of Figure 12 suggests that the position of the VBM has little to no

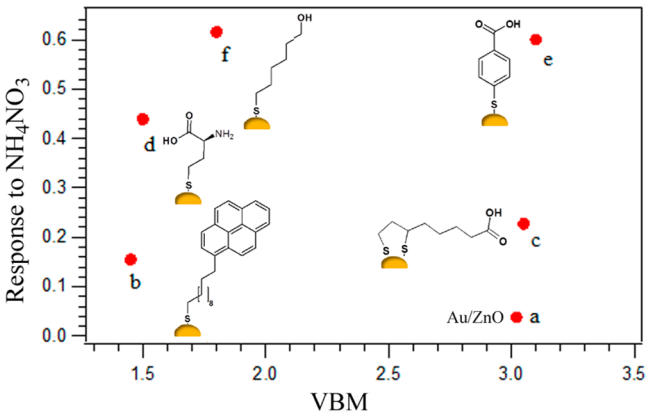

Figure 12. Samples responses to ammonium nitrate exposure versus the position of their respective VBM. (a) Untreated Au/ZnO nanospring-mat and samples treated with (b) 11-(1-pyrenyl)-1-undecathiol, (c) DL-thioctic acid, (d) L-cysteine, (e) 4-mercaptobenzoic acid, and (f) 6-mercaptohexanol.

influence in the response to vapors of ammonium nitrate. The magnitude of the responses of the sensors appears to reflect the packing density and/or ordering of thiols, as determined from the XPS analysis. However, given the dissimilarity of the five thiols, one has to assume that chemical interactions also play an important role in sensing.

Chemical Interactions between Functional Groups of Receptors and Explosive Vapors. Ammonium nitrate (NH_4NO_3) decomposes into ammonia (NH_3) and oxidizing nitric acid (HNO_3), and gaseous degradation products (N_2, H_2O, O_2, OH, HNO, and NO_3).[50] Receptors with carboxylic acid groups (L-cysteine, 4-mercaptobenzoic acid, DL-thioctic acid) may interact with ammonium (NH_4^+) through electrostatic interactions and with NH_3 via hydrogen bonding. On the

dx.doi.org/10.1021/am504371k | ACS Appl. Mater. Interfaces 2014, 6, 13355−13366

other hand, receptors with alcohol or amino groups (6-mercaptohexanol, L-cysteine) should only interact via hydrogen bonds. The polarized nitro groups ($R\text{-}NO_2$) found in many commonly used military explosives are known to interact strongly with polar groups, such as −COOH and −OH via ionic and hydrogen bond interactions. Thus, all of the receptors, except for 11-(1-pyrenyl)-1-undecathiol, may interact strongly with nitrate ions (NO_3^-). The sensor data (Figure 12), with the exception of DL-thioctic acid and 6-mercaptohexanol, are in good agreement with the above description of chemical interactions between functional groups of receptors and vapors of ammonium nitrate. The reversibility of the 6-mercaptohexanol functionalized sensors does not support the assumption that there is strong interaction with the analytes. In fact, diffusion of the analytes into the 6-mercaptohexanol SAM better explains its reversible characteristics. 4-mercaptobenzoic acid and L-cysteine respond better, whereas the response is low for 11-(1-pyrenyl)-1-undecathiol. The former have polar linker headgroups of the form −COOH, −OH, and $-NH_2$ that interact with components from ammonium nitrate, while the latter does not. However, DL-thioctic acid, which has the polar linker −COOH headgroup, exhibits a relatively lower response. The characterization data already showed that the surface energy barrier is relatively high for DL-thioctic acid treated samples. From a chemical standpoint, the low response could be attributable to poor long-range order of the DL-thioctic acid SAM.[51]

4. SUMMARY

The electronic structure of alkyl thiol-functionalized Au/ZnO nanosprings have been characterized with XPS and UPS and correlated to the response of corresponding chemical sensors with exposures to ammonium nitrate, a chemical signature of more common explosives. The thiols used in the study were L-cysteine, 6-mercaptohexanol, 11-(1-pyrenyl)-1-undecathiol, 4-mercaptobenzoic acid, and DL-thioctic acid. XPS analysis revealed that the thiols' headgroups are located at the SAMs-air interface and are resistant to oxidation. The weakness of the S 2p core level intensities of 4-mercaptobenzoic acid and 11-(1-pyrenyl)-1-undecathiol functionalized samples suggests that the effects of steric screening on the inelastic scattering of photoelectrons is significant. XPS analysis of the C/S ratios of the adsorbed thiols at room temperature, as well as at the temperatures at which the sensors are operated, confirmed that they remain intact. The analysis of the UPS valence band spectra of the thiolated samples exhibited contributions from the molecular orbitals of the thiols, S−Au and S−Zn bonding, the Au/ZnO nanospring substrate, and attenuation of some substrate bands due to thiol induced scattering. UPS difference spectra revealed bands associated with carbon 2p and nitrogen 2p states, and more importantly, with S−Au bonding and antibonding orbitals of both π- and σ-type. The formation of hybrid orbitals of both antibonding and bonding type above and below the metal d-bands is characteristic of molecular chemisorption on metal surfaces.

Vapor-sensing tests show that the thiols are more thermally stable on Au/ZnO nanosprings than on Au thin films. It is hypothesized that coadsorption to the ZnO surface is responsible for their enhanced stability. All of the thiolated sensors are highly responsive to vaporized ammonium nitrate. Au/ZnO nanosprings with SAMs of 6-mercaptohexanol or 4-mercaptobenzoic acid exhibited the strongest responses with four and five orders of magnitude change in conductance, respectively. It is hypothesized that the strong response for 6-mercaptohexanol, as well as its self-refreshing capability, is due to the high packing density and ordering of the SAM, which enables the analyte to diffuse in and out the SAM. If correct, the development of protocols that maximize long-range order of SAMs layers are in order as a means for producing sensitive, self-refreshing, explosive sensors.

■ ASSOCIATED CONTENT

Supporting Information

Electron flood gun parameters during irradiation of the samples. Thermal stability of thiols on Au/ZnO nanosprings Synthesis of 11-(1-pyrenyl)-1-undecathiol scheme and corresponding NMR spectra. These materials are available free of charge via Internet at http://pubs.acs.org.

■ AUTHOR INFORMATION

Corresponding Authors

*E-mail: dmcilroy@uidaho.edu.
*E-mail: foue3398@vandals.uidaho.edu

Notes

The authors declare no competing financial interest.

■ ACKNOWLEDGMENTS

The authors express their sincere appreciation to Dr T. Williams for his kind assistance with FESEM, TEM and XRD. This research was financially supported by The Office of Naval Research (Research Opportunity Number ONR BAA 09-022). D.N.M.acknowledges the support of the College of Science's Dyess Faculty Fellowship.

■ REFERENCES

(1) Singh, S. Sensors—An Effective Approach for the Detection of Explosives. *J. Hazard. Mater.* **2007**, *144*, 15−28.
(2) Senesac, L.; Thundat, T. G. Nanosensors for Trace Explosive Detection. *Mater. Today* **2008**, *11*, 28−36.
(3) Dobrokhotov, V.; Oakes, L.; Sowell, D.; Larin, A.; Hall, J.; Kengne, A.; Bakharev, P.; Corti, G.; Cantrell, T.; Prakash, T.; et al. Toward the Nanospring-Based Artificial Olfactory System for Trace-Detection of Flammable and Explosive Vapors. *Sens. Actuators, B* **2012**, *168*, 138−148.
(4) Dasary, S. S. R.; Singh, A. K.; Senapati, D.; Yu, H.; Ray, P. C. Gold Nanoparticle Based Label-Free SERS Probe for Ultrasensitive and Selective Detection of Trinitrotoluene. *J. Am. Chem. Soc.* **2009**, *131*, 13806−13812.
(5) Capua, E.; Cao, R.; Sukenik, C. N.; Naaman, R. Detection of Triacetone Triperoxide (TATP) with an Array of Sensors Based on Non-Specific Interactions. *Sens. Actuators, B* **2009**, *140*, 122−127.
(6) Goodpaster, J. V.; McGuffin, V. L. Fluorescence Quenching as an Indirect Detection Method for Nitrated Explosives. *Anal. Chem.* **2001**, *73*, 2004−2011.
(7) Joseph, Y.; Besnard, I.; Rosenberger, M.; Guse, B.; Nothofer, H.-G.; Wessels, J. M.; Wild, U.; Knop-Gericke, A.; Su, D.; Schlögl, R.; et al. Self-Assembled Gold Nanoparticle/Alkanedithiol Films: Preparation, Electron Microscopy, XPS-Analysis, Charge Transport, and Vapor-Sensing Properties. *J. Phys. Chem. B* **2003**, *107*, 7406−7413.
(8) Dobrokhotov, V.; McIlroy, D. N.; Norton, M. G.; Abuzir, A.; Yeh, W. J.; Stevenson, I.; Pouy, R.; Bochenek, J.; Cartwright, M.; Wang, L.; et al. Principles and Mechanisms of Gas Sensing by GaN Nanowires Functionalized with Gold Nanoparticles. *J. Appl. Phys.* **2006**, *99*, 104302.
(9) Dobrokhotov, V.; Oakes, L.; Sowell, D.; Larin, A.; Hall, J.; Kengne, A.; Bakharev, P.; Corti, G.; Cantrell, T.; Prakash, T.; et al. ZnO Coated Nanospring-Based Chemiresistors. *J. Appl. Phys.* **2012**, *111*, 044311.

(10) Wang, L.; Major, D.; Paga, P.; Zhang, D.; Norton, M. G.; McIlroy, D. N. High Yield Synthesis and Lithography of Silica-Based Nanospring Mats. *Nanotechnology* **2006**, *17*, S298−S303.
(11) Castner, D. G.; Hinds, K.; Grainger, D. W. X-Ray Photoelectron Spectroscopy Sulfur 2p Study of Organic Thiol and Disulfide Binding Interactions with Gold Surfaces. *Langmuir* **1996**, *12*, 5083−5086.
(12) Bain, C. D.; Troughton, E. B.; Tao, Y. T.; Evall, J.; Whitesides, G. M.; Nuzzo, R. G. Formation of Monolayer Films by the Spontaneous Assembly of Organic Thiols from Solution onto Gold. *J. Am. Chem. Soc.* **1989**, *111*, 321−335.
(13) Watts, J. F. *An Introduction to Surface Analysis by XPS and AES*; J. Wiley: Chichester, U.K., 2003.
(14) Scott, A.; Janes, D. B. Characterization of Electrochemically Grafted Molecular Layers on Silicon for Electronic Device Applications. *J. Appl. Phys.* **2009**, *105*, 073512.
(15) Libertino, S.; Scandurra, A.; Aiello, V.; Giannazzo, F.; Sinatra, F.; Renis, M.; Fichera, M. Layer Uniformity in Glucose Oxidase Immobilization on SiO2 Surfaces. *Appl. Surf. Sci.* **2007**, *253*, 9116−9123.
(16) Abdureyim, A.; Okudaira, K. K.; Harada, Y.; Masuda, S.; Aoki, M.; Seki, K.; Ito, E.; Ueno, N. Characterization of 4-Mercaptohydrocynnamic Acid Self-Assembled Film on Au(111) by Means of X-Ray Photoelectron Spectroscopy. *J. Electron Spectrosc. Relat. Phenom.* **2001**, *114*−*116*, 371−374.
(17) Moulder, J. F.; Stickle, W. F.; Sobol, P. E.; Bomben, K. D. *Handbook of X-Ray Photoelectron Spectroscopy*; Perkin-Elmer Corporation, Physical Electronics Division: Eden Prairie, MN, 1995; p 55344.
(18) Sadik, P. W.; Pearton, S. J.; Norton, D. P.; Lambers, E.; Ren, F. Functionalizing Zn- and O-Terminated ZnO with Thiols. *J. Appl. Phys.* **2007**, *101*, 104514.
(19) Singh, J.; Im, J.; Whitten, J. E.; Soares, J. W.; Steeves, D. M. Chemisorption of a Thiol-Functionalized Ruthenium Dye on Zinc Oxide Nanoparticles: Implications for Dye-Sensitized Solar Cells. *Chem. Phys. Lett.* **2010**, *497*, 196−199.
(20) Chen, J.; Ruther, R. E.; Tan, Y.; Bishop, L. M.; Hamers, R. J. Molecular Adsorption on ZnO($10\bar{1}0$) Single-Crystal Surfaces: Morphology and Charge Transfer. *Langmuir* **2012**, *28*, 10437−10445.
(21) Singh, J.; Im, J.; Watters, E. J.; Whitten, J. E.; Soares, J. W.; Steeves, D. M. Thiol Dosing of ZnO Single Crystals and Nanorods: Surface Chemistry and Photoluminescence. *Surf. Sci.* **2013**, *609*, 183−189.
(22) LaLonde, A. D.; Norton, M. G.; Zhang, D.; Gangadean, D.; Alkhateeb, A.; Padmanabhan, R.; McIlroy, D. N. Controlled Growth of Gold Nanoparticles on Silica Nanowires. *J. Mater. Res.* **2005**, *20*, 3021−3027.
(23) Turba, T.; Norton, M. G.; Niraula, I.; McIlroy, D. N. Ripening of Nanowire-Supported Gold Nanoparticles. *J. Nanopart. Res.* **2009**, *11*, 2137−2143.
(24) Kuo, F.-L.; Li, Y.; Solomon, M.; Du, J.; Shepherd, N. D. Workfunction Tuning of Zinc Oxide Films by Argon Sputtering and Oxygen Plasma: An Experimental and Computational Study. *J. Phys. D: Appl. Phys.* **2012**, *45*, 065301.
(25) Heinhold, R.; Williams, G. T.; Cooil, S. P.; Evans, D. A.; Allen, M. W. Influence of Polarity and Hydroxyl Termination on the Band Bending at ZnO Surfaces. *Phys. Rev. B* **2013**, *88*, 235315.
(26) Islam, M. N.; Ghosh, T. B.; Chopra, K. L.; Acharya, H. N. XPS and X-Ray Diffraction Studies of Aluminum-Doped Zinc Oxide Transparent Conducting Films. *Thin Solid Films* **1996**, *280*, 20−25.
(27) Powel, C. J.; Jablonski, A. *NIST Electron Inelastic-Mean -Free-Path Datbase*, Version 1.2, SRD71; National Institute of Standards and Tectnology: Gaitherburg, MD, 2010.
(28) Yeh, J. J.; Lindau, I. Atomic Subshell Photoionization Cross Sections and Asymmetry Parameters: $1 \leqslant Z \leqslant 103$. *At. Data Nucl. Data Tables* **1985**, *32*, 1−155.
(29) Guglieri, C.; Chaboy, J. Characterization of the ZnO−ZnS Interface in THIOL-Capped ZnO Nanoparticles Exhibiting Anomalous Magnetic Properties. *J. Phys. Chem. C* **2010**, *114*, 19629−19634.
(30) Guglieri, C.; Laguna-Marco, M. A.; García, M. A.; Carmona, N.; Céspedes, E.; García-Hernández, M.; Espinosa, A.; Chaboy, J. XMCD Proof of Ferromagnetic Behavior in ZnO Nanoparticles. *J. Phys. Chem. C* **2012**, *116*, 6608−6614.
(31) Guglieri, C.; Espinosa, A.; Carmona, N.; Laguna-Marco, M. A.; Céspedes, E.; Ruíz-González, M. L.; González-Calbet, J.; García-Hernández, M.; García, M. A.; Chaboy, J. Relationship between the Magnetic Properties and the Formation of a ZnS/ZnO Interface in S-Capped ZnO Nanoparticles and ZnS−ZnO Thin Films. *J. Phys. Chem. C* **2013**, *117*, 12199−12209.
(32) Volkert, A. A.; Subramaniam, V.; Ivanov, M. R.; Goodman, A. M.; Haes, A. J. Salt-Mediated Self-Assembly of Thioctic Acid on Gold Nanoparticles. *ACS Nano* **2011**, *5*, 4570−4580.
(33) Schlenoff, J. B.; Li, M.; Ly, H. Stability and Self-Exchange in Alkanethiol Monolayers. *J. Am. Chem. Soc.* **1995**, *117*, 12528−12536.
(34) Barriet, D.; Yam, C. M.; Shmakova, O. E.; Jamison, A. C.; Lee, T. R. 4-Mercaptophenylboronic Acid SAMs on Gold: Comparison with SAMs Derived from Thiophenol, 4-Mercaptophenol, and 4-Mercaptobenzoic Acid. *Langmuir* **2007**, *23*, 8866−8875.
(35) Wells, M.; Dermody, D. L.; Yang, H. C.; Kim, T.; Crooks, R. M.; Ricco, A. J. Interactions between Organized, Surface-Confined Monolayers and Vapor-Phase Probe Molecules. 9. Structure/Reactivity Relationship between Three Surface-Confined Isomers of Mercaptobenzoic Acid and Vapor-Phase Decylamine. *Langmuir* **1996**, *12*, 1989−1996.
(36) Sharma, M. K.; Rao, V. K.; Merwyn, S.; Agarwal, G. S.; Upadhyay, S.; Vijayaraghavan, R. A Novel Piezoelectric Immunosensor for the Detection of Malarial Plasmodium Falciparum Histidine Rich Protein-2 Antigen. *Talanta* **2011**, *85*, 1812−1817.
(37) Li, Z.; Niu, T.; Zhang, Z.; Feng, G.; Bi, S. Studies on the Effect of Solvents on Self-Assembly of Thioctic Acid and Mercaptohexanol on Gold. *Thin Solid Films* **2011**, *519*, 4225−4233.
(38) Bensebaa, F.; Ellis, T. H.; Badia, A.; Lennox, R. B. Thermal Treatment of *n* -Alkanethiolate Monolayers on Gold, As Observed by Infrared Spectroscopy. *Langmuir* **1998**, *14*, 2361−2367.
(39) Zhang, J.; Chi, Q.; Nielsen, J. U.; Friis, E. P.; Andersen, J. E. T.; Ulstrup, J. Two-Dimensional Cysteine and Cystine Cluster Networks on Au(111) Disclosed by Voltammetry and in Situ Scanning Tunneling Microscopy. *Langmuir* **2000**, *16*, 7229−7237.
(40) Scudiero, L.; Hipps, K. W.; Barlow, D. E. A Self-Organized Two-Dimensional Bimolecular Structure. *J. Phys. Chem. B* **2003**, *107*, 2903−2909.
(41) Henrich, V. E.; Cox, P. A. *The Surface Science of Metal Oxides*; Cambridge University Press: Cambridge, U.K., 1994.
(42) Duwez, A.-S.; Pfister-Guillouzo, G.; Delhalle, J.; Riga, J. Probing Organization and Structural Characteristics of Alkanethiols Adsorbed on Gold and of Model Alkane Compounds through Their Valence Electronic Structure: An Ultraviolet Photoelectron Spectroscopy Study. *J. Phys. Chem. B* **2000**, *104*, 9029−9037.
(43) Alloway, D. M.; Hofmann, M.; Smith, D. L.; Gruhn, N. E.; Graham, A. L.; Coloradp, R., Jr.; Wysocki, V. H.; Lee, T. R.; Lee, P. A.; Armstrong, N. Interface Dipoles Arising from Self-Assembled Monolayers on Gold: UV-Photoemission Studies of Alkanethiols and Partially Fluorinated Alkanethiols. *J. Phys. Chem. B* **2003**, *107*, 11690−11699.
(44) Göpel, W.; Bauer, R. S.; Hansson, G. Ultraviolet Photoemission Studies of Chemisorption and Point Defect Formation on ZnO Nonpolar Surfaces. *Surf. Sci.* **1980**, *99*, 138−156.
(45) Von Wrochem, F.; Gao, D.; Scholz, F.; Nothofer, H.-G.; Nelles, G.; Wessels, J. M. Efficient Electronic Coupling and Improved Stability with Dithiocarbamate-Based Molecular Junctions. *Nat. Nanotechnol.* **2010**, *5*, 618−624.
(46) North Atlantic Treaty Organization; NATO Advanced Study Institute on Chemisorption and Reactivity on Supported Clusters and Thin Films: Towards an Understanding of Microscopic Processes in Catalysis. *Chemisorption and Reactivity on Supported Clusters and Thin Films: Towards an Understanding of Microscopic Processes in Catalysis*; NATO ASI series. Series E, Applied sciences; Kluwer Academic Publishers: Dordrecht, The Netherlands, 1997.

(47) Di Felice, R.; Selloni, A.; Molinari, E. DFT Study of Cysteine Adsorption on Au(111). *J. Phys. Chem. B* **2003**, *107*, 1151−1156.
(48) Rubloff, G. W.; Lüth, H.; Grobman, W. D. Orbital Energy Shifts Associated with Chemical Bonding of Organic Molecules on ZnO Nonpolar Surfaces. *Chem. Phys. Lett.* **1976**, *39*, 493−496.
(49) Dobrokhotov, V.; Oakes, L.; Sowell, D.; Larin, A.; Hall, J.; Barzilov, A.; Kengne, A.; Bakharev, P.; Corti, G.; Cantrell, T.; et al. Thermal and Optical Activation Mechanisms of Nanospring-Based Chemiresistors. *Sensors* **2012**, *12*, 5608−5622.
(50) Cagnina, S.; Rotureau, P.; Fayet, G.; Adamo, C. The Ammonium Nitrate and Its Mechanism of Decomposition in the Gas Phase: A Theoretical Study and a DFT Benchmark. *Phys. Chem. Chem. Phys.* **2013**, *15*, 10849.
(51) Willey, T. M.; Vance, A. L.; Bostedt, C.; van Buuren, T.; Meulenberg, R. W.; Terminello, L. J.; Fadley, C. S. Surface Structure and Chemical Switching of Thioctic Acid Adsorbed on Au(111) As Observed Using Near-Edge X-Ray Absorption Fine Structure. *Langmuir* **2004**, *20*, 4939−4944.